# EXPERIMENTAL AND NUMERICAL STUDY OF DEBONDING IN COMPOSITE ADHESIVE JOINTS

**Rosen T. Tenchev, Brian G. Falzon**
**Imperial College, London, UK**

**Keywords**: *interface elements, decohesive zone, mixed mode, DCB, ELST*

***Abstract***

*The mode I and mode II fracture properties of the FM300-2 adhesive bond between 5HS/RTM6 laminates are determined experimentally by DCB and ELS test.*

*The crack propagation is studied numerically by means of interface elements based on the decohesive zone model. The latter is characterized by material degradation, which is usually assumed to be linear. In the present study it is shown that if a non-linear material degradation is used with an increased magnitude of the interface relative displacement at failure it is possible to model more correctly the experimentally observed significant non-linear behaviour before the start of crack propagation.*

*An adhesive stepped flush joint is studied experimentally and numerically. A mixed mode interaction criterion is used together with the non-linear material degradation of the interface. Sensitivity studies are performed to study the influence of the parameters defining it.*

## 1 Introduction

Experimental studies have shown that an adhesive stepped flush joint may decrease the load carrying capacity by up to 40% [1]. The failure mode is a combination of adhesive failure and composite adhesive surface debonding. Since the adhesive layer is very thin, compared to a typical laminate thickness, the failure process can be modelled as a crack propagation problem. An established numerical strategy is to make use of an interface finite element that is based on the decohezive zone approach [2].

In this paper the identification of certain parameters of the interface element constitutive law, related to the decohesive zone, is discussed. This enables the finite element analysis to predict more accurately the experimentally observed non-linear behaviour at the initiation of crack propagation. The non-linear interface constitutive law is used to analyse a stepped flush joint.

## 2 Fracture Properties - Experimental Studies

The crack propagation through an adhesive bond was studied for mode I on double cantilever beam (DCB) specimens, and for mode II – on end load split (ELS) specimens [3].

### 2.1 Mode I, DCB test

The loading and deformation of a DCB specimen are shown in Fig. 1. The dimension, in *mm*, are: $L$=140.0, $B$=20.0, $h$=2.9, $c$=19.0, $a_0$=30.0 The separation $d$ of the cantilever arms is measured by an LVDT. Graph paper was bonded along the length of the adhesive interface to measure the propagation of the crack. The latter was observed and recorded by a travelling zoom camera. Still shots of the crack propagation for one specimen are presented in Fig. 2. It can be seen that the crack grows either by a single crack propagation or the propagation and coalescence of several cracks.

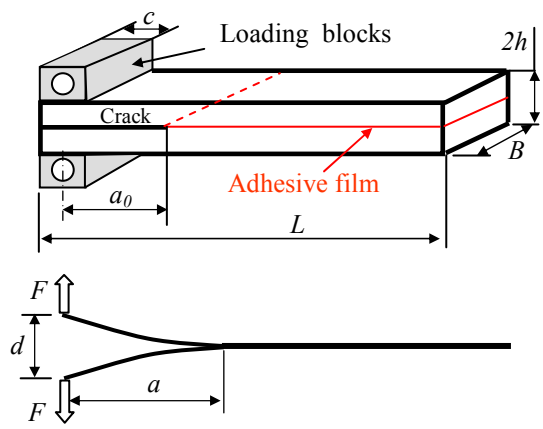


Fig. 1. DCB test. Specimen and free body diagram.

It was observed that the crack patterns at the front and back surfaces are not the same, which means that the crack front is not a straight line and it may not traverse the whole width of the specimen. To model the decrease of the stiffness of the adhesive interface these patches can be smeared into a softening decohesive zone.

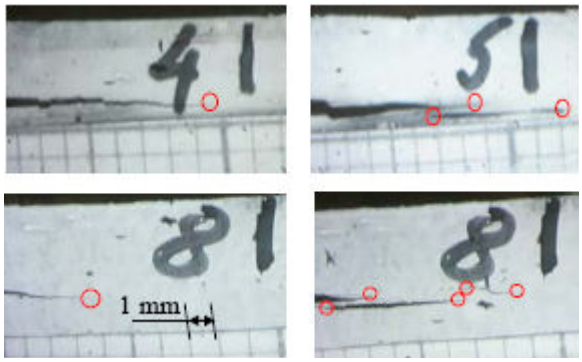


**Single crack front** **Multi fronts: a decohesive zone.**

Fig. 2. DCB tests. Crack propagation.

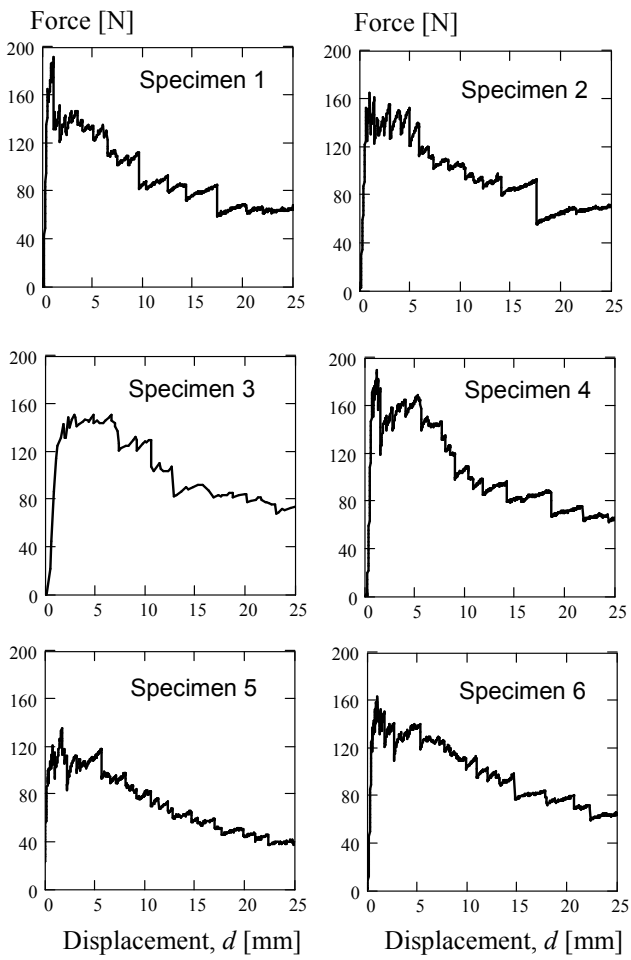


Fig. 3. DCB tests. Force-displacement response.

The measured force-displacement response during crack propagation of six specimens is shown in Fig. 3. The graphs are not smooth because the crack propagates in discrete steps.

The crack length growth is visually recorded together with the force-displacement measurement display. Based on beam theory [3] the energy release rate $G_{Ic}$ can be computed by three formulas, Eqs. 1. Analytically the three variables (force $F$, displacement $d$, and crack length $a$) are not independent and the formulas will give the same results for $G_{Ic}$.

$$G_{Ic} = \frac{1}{B}\frac{(Fa)^2}{EI} \tag{1a}$$

$$G_{Ic} = \frac{3}{2}\frac{1}{B}\frac{Fd}{a} \tag{1b}$$

$$G_{Ic} = \frac{1}{B}\left[\frac{F^2 d}{\frac{2}{3}\sqrt{EI}}\right]^{\frac{2}{3}} \tag{1c}$$

The laminate's elastic modulus in bending was experimentally determined on intact cantilever specimen to be $E_b = 36\ GPa$.

Various techniques for correcting beam theory (compliance corrections for root rotation, large displacements, etc., [4]) were considered but the change in the results was insignificant when compared to the large oscillations in Fig. 3. The factor that had the biggest influence (but still less than 3%) was the change of the force moment arm due to the rotation of the loading blocks. Hence all these corrections are omitted here for simplicity.

The energy release rates are computed by Eq. 1a, 1b and 1c and the results for four specimens are presented in Fig. 4. The results computed by the three formulas are averaged. These averaged results are linearly interpolated (because for each specimen the recorded data is for different $d$ and $F$) and averaged again. The final resistance $R$ curve is presented in Fig. 5. A steady state value of $G_{Ic}$ = 1.33 [$N/mm$] is well defined. The crack initiation value is lower ($G_{Ic,0}$ =0.62 $N/mm$), which agrees with other experimental data [5].

## 2.2 Mode II, ELS test

The same specimen, shown in Fig. 1, is used for mode II ELS tests. The loading and the supports are according to the free body diagram shown in Fig. 6. Five specimens were tested: three with initial crack length $a_0$=30 mm; one with $a_0$=40 mm and one

with $a_0$=50 mm. The force displacement ($F$-$d$) graphs are shown in Fig. 7.

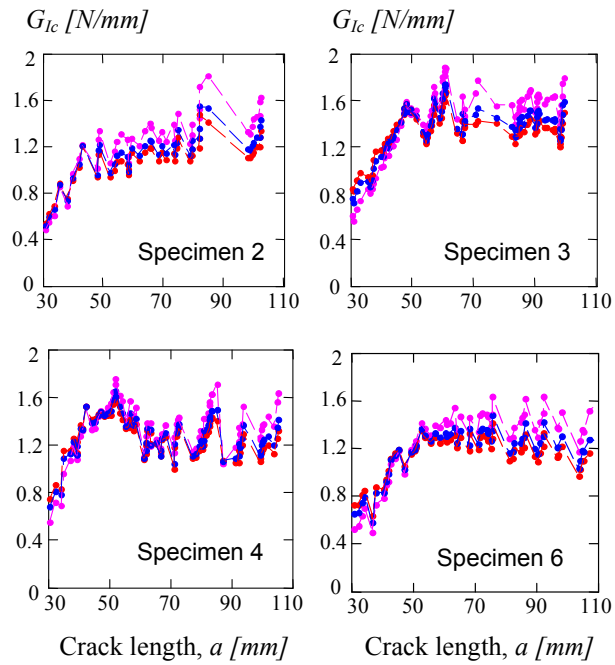


Fig. 4. $G_{Ic}$ computed by Eqs 1a, 1b and 1c.

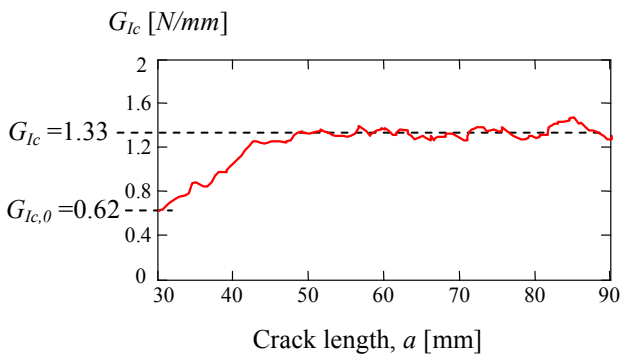


Fig. 5. Fracture toughness $G_{Ic}$, $R$ curve.

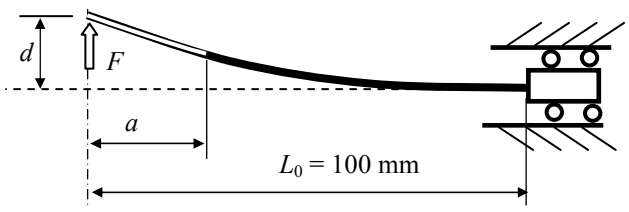


Fig. 6. ELS test. Free body diagram.

The equations for computing the energy release rate $G_{IIc}$ , derived from beam theory [3], are:

$$G_{IIc} = \left\{ \left( d - \frac{FL^3}{2\,EBh^3} \right) \left[ \frac{9}{4} \left( \frac{B}{F} \right)^2 \sqrt{Eh^3} \right]^{-1} \right\}^{\frac{2}{3}} \tag{2a}$$

$$G_{IIc} = \frac{9}{4\,Eh^3} \left( \frac{Fa}{B} \right)^2 \tag{2b}$$

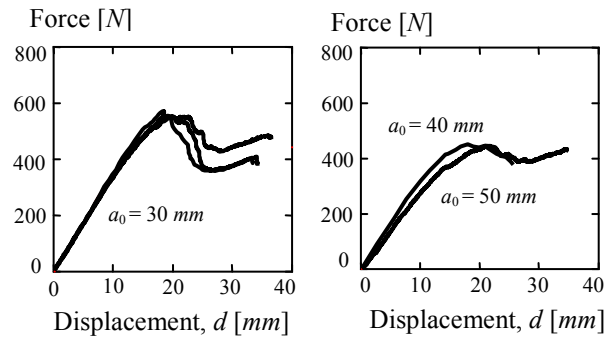


Fig. 7. ELS test. Force-displacement response.

The results based on Eq. 2a for the five tested specimens are plotted in Fig. 8a. The $R$ curve, after the two step averaging used in the previous section (i.e. averaging results from Eq. 2a and Eq. 2b for all specimen and then averaging the interpolated curves) is plotted in Fig. 8b.

The basic differences between the experimental mode II results and mode I is that the mode II force-displacement response show less oscillations but there is no well defined 'plateau' value for $G_{IIc}$. The reason for this is most probably the friction forces and a possible interlocking of the exposed fiber bundles along the already delaminated crack surfaces. A value for $G_{IIc}$ between 5 and 6 [$N/mm$], based on the graphs in Fig. 8a, will be used in later analytical and numerical calculations. The energy release rate at crack initiation is estimated to be $G_{IIc,0}$=1.15 $N/mm$.

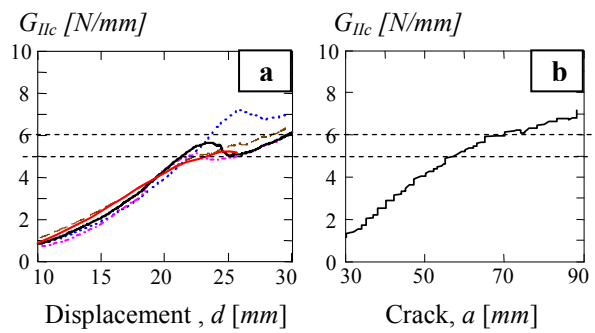


Fig. 8. ELS test. Energy release rate $G_{II,c}$

### 2.3 Experimental v. beam theory results

In Fig. 5 and Fig. 8 it can be seen that during the initial stages of crack propagation the energy release rates depend on the crack length. In analytical and numerical analysis $G_{I,c}$ and $G_{II,c}$ are defined as material properties independent of any geometry dimensions. How well the analytical beam theory solution matches the experimental results, when constant values for $G_{I,c}$ and $G_{II,c}$ are used, is presented in Fig. 9. It can be seen that there is good agreement during the crack propagation but the non-linear behaviour shown during the initiation of crack growth cannot be modeled accurately.

The finite element interface elements, used in the analyses, are based on the concept of a decohesive zone. The physical existence of such zone can be deduced from the multicrack pattern in Fig. 2. If suitable parameters that define the decohesive zone are used, it is possible to improve on the numerical prediction of crack growth initiation.

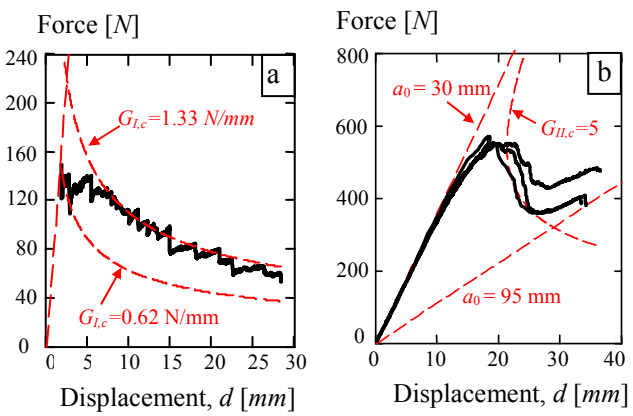


Fig. 9. Experimental (solid black line) and beam theory (broken red line) results.
(a) Mode I, DCB test; (b) Mode II, ELS test.

### 3. Interface elements

A 2D interface element [6, 7] is shown in Fig. 10. It has either two or three pairs of nodes depending on whether it connects linear or quadratic elements, respectively. It has zero thickness $h$ so nodes 1 and 3 have identical coordinates and similarly for nodes 2 and 4. Each node has two degrees of freedom, normal and tangential. The relative displacements $\delta_I = \mathrm{v}_{top} - \mathrm{v}_{bot}$ and $\delta_{II} = u_{top} - u_{bot}$ represent delamination in mode I and mode II, respectively. The bond between a node pair of the interface is completely severed when the energy accumulated during their relative displacement reaches the critical energy release rate $G_c$

$$G_c = \int_0^{\delta_c} \sigma d\delta \qquad (3)$$

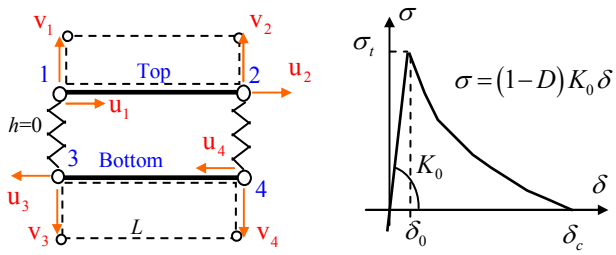


Fig. 10. Interface finite element and its constitutive law

The initial 'penalty' stiffness $K_0 = \sigma_t / \delta_0$ has to be sufficiently large to correctly model the pre-delamination response as well as to enforce the 'no penetration' condition when the relative displacement is in a closing mode. The interface constitutive law is usually assumed to be bilinear. Other formulations, with a smooth transition at $\sigma_t$ to avoid numerical problems, have been also used [8]. The shape of the softening curve and the magnitude of the critical relative displacement $\delta_c$ (provided that the area below the curve remains equal to $G_c$) have no influence on the prediction of the crack propagation. Small values of $\delta_c$ are used when results are checked against analytical beam theory solutions, which does not consider decohesive softening. Experimental data shows a significant non-linear behaviour just before the initiation of crack propagation, Fig. 9, which can be explained by the development of an extensive decohesive zone. In the present study it will be shown how modifying the magnitude of the critical relative displacement $\delta_c$ and the shape of the softening curve, while regarding $G_c$ as constant material property, can improve the numerical modeling of the crack propagation initiation and subsequent growth.

To study the delamination initiation and propagation, a finite element software has been developed by the authors. It is based on a pseudo-transient formulation [7], which uses the secant

stiffness modulus and avoids spurious oscillations in the solutions [6], typical of other more conventional solution strategies.

### 3.1 Interface constitutive law

The strain softening interface constitutive relationship, for mode I as well as mode II, may be given by a power law

$$\sigma(\delta)=\begin{cases}\dfrac{\sigma_t}{\delta_0}\delta & if \quad \delta\le\delta_0\\ \sigma_t\left[1-\left(\dfrac{\delta}{\delta_C}\right)^k\right] & if \quad \delta_0<\delta<\delta_c\\ 0 & if \quad \delta\ge\delta_c\end{cases} \tag{4}$$

The energy release rate, when the energy of the elastic deformation is ignored (i.e. $\delta_0$ =0 since $\delta_0 \ll \delta_c$), is:

$$G_c=\frac{1}{2}\sigma_t\delta_0+\frac{k}{k+1}\sigma_t\left(\delta_c-\delta_0\right)\approx\frac{k}{k+1}\sigma_t\delta_c \tag{5}$$

## 4. Comparison of FE and experimental results

Finite element analyses (FEA), using the experimental values for the critical energy release rates, have been carried out to determine the most suitable values for $k$ and $\delta_c$ in Eq. 4 and Eq. 5).

Comparisons of the experimental results with the corresponding FEA results and beam theory results are presented in Fig. 11 and Fig. 12 for the DCB and ELS test, respectively.

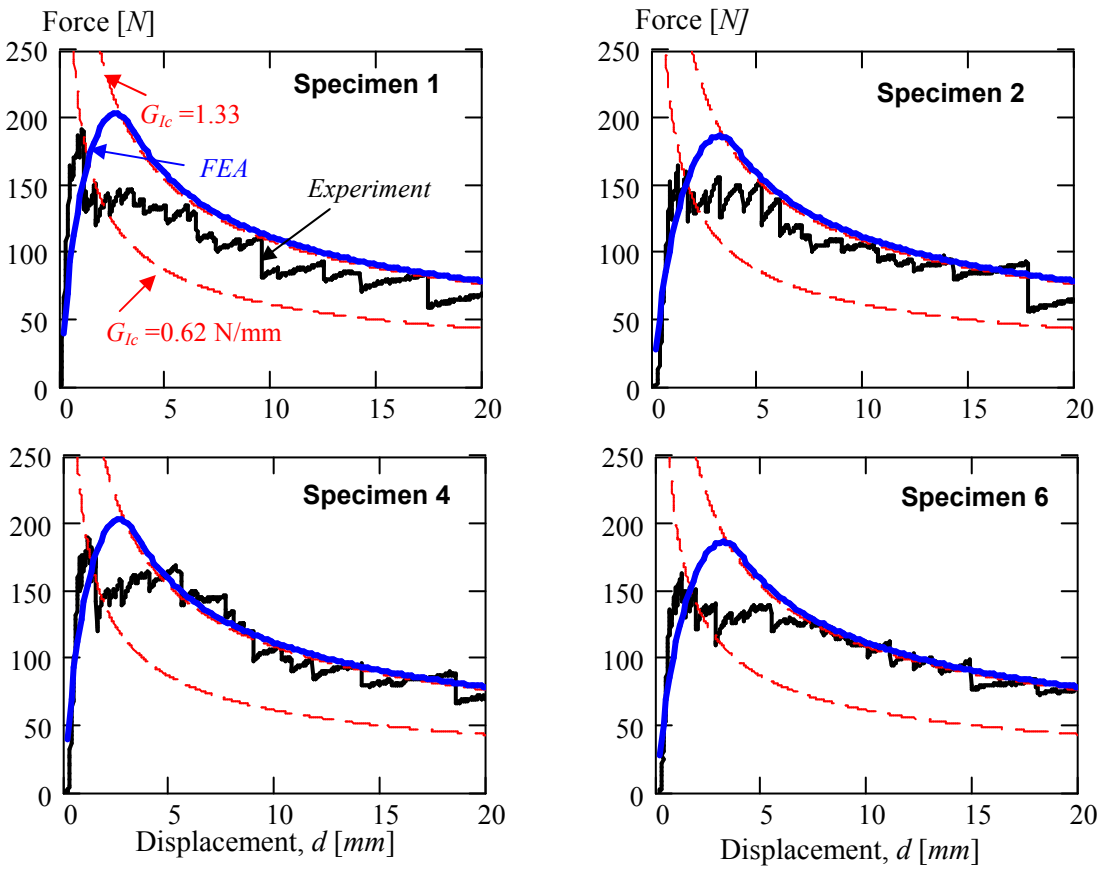


Fig. 11 DCB mode I tests.

**Black** line – Experimental results,
Red dash lines – Beam theory results, $G_{Ic}$ =0.62 and $G_{Ic}$ =1.33 *N/mm*
**Blue** line – Finite element results, $G_{Ic}$ =1.33 *N/mm*

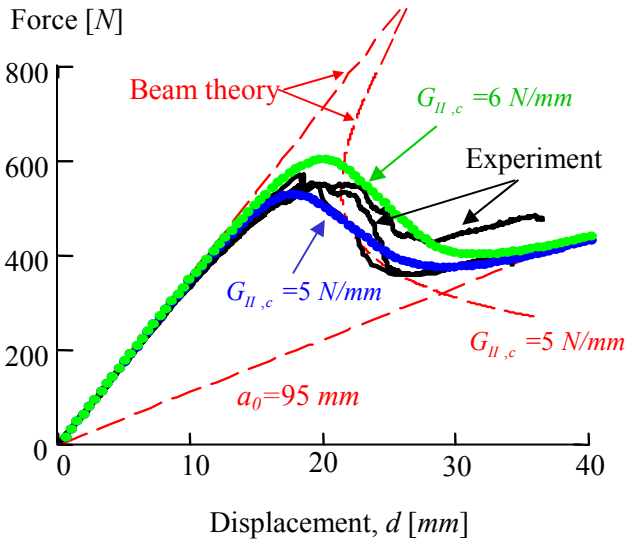


Fig. 12. ELS mode II tests.

**Black** line – Experimental results,
Red dash lines – Beam theory results,
**Blue**, **Green** line – Finite element results.

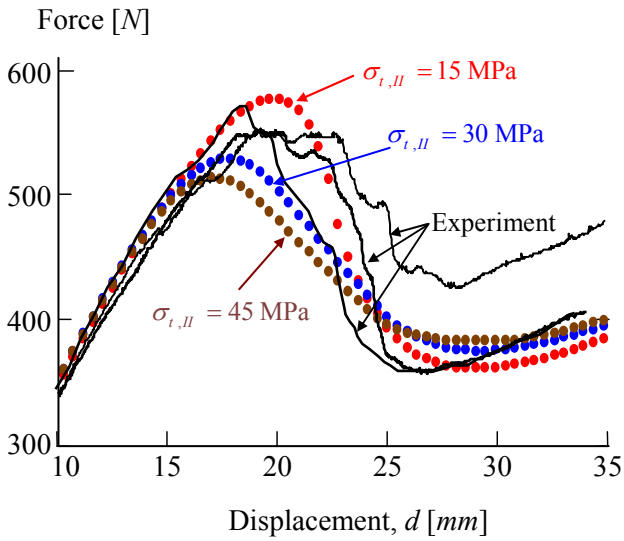


Fig. 13. ELS tests. Influence of $\delta_{II,c}$ and $k$.

$\sigma_{t,II}$ = 15 MPa : $\delta_{II,c}$ = 0.67 *mm*; $k$ = 1.00
$\sigma_{t,II}$ = 30 MPa : $\delta_{II,c}$ = 1.00 *mm*; $k$ = 0.20
$\sigma_{t,II}$ = 45 MPa : $\delta_{II,c}$ = 1.12 *mm*; $k$ = 0.11

The fracture toughnesses are determined from the experimental data, Fig. 5 and Fig. 8. The power law coefficient $k$ and the relative displacements at failure $\delta_{I,c}$ and $\delta_{II,c}$ are determined to best fit the experimental results, Fig. 3 and Fig. 7. The interface strength $\sigma_{t,I}$ and $\sigma_{t,II}$ are computed from Eq. 5. They should be regarded as the interface strength, in the corresponding mode, of the adhesive bond system: composite laminate *5HS/RTM6* and adhesive *FM300-2*.

The set of the interface material properties, used in the analyses, is given in Table 1.

In Fig. 12 the line '$a_0$= 95*mm*' stands for beam theory results at full delamination. Since the experimental results, Fig. 8, does not show a well defined stationary value for the fracture toughness FEA results with $G_{IIc}$ =5.0 *N/mm* and $G_{IIc}$ =6.0 *N/mm* have been computed to show a range of acceptable values for $G_{IIc}$.

Table 1. Interface material properties

| $G_{Ic}$ *N/mm* | $G_{IIc}$ *N/mm* | $\sigma_{t,I}$ *MPa* | $\sigma_{t,II}$ *MPa* | $\delta_{I,c}$ *mm* | $\delta_{II,c}$ *mm* | $k$ |
|---|---|---|---|---|---|---|
| 1.33 | 5.0 | 8.0 | 30.0 | 1.0 | 1.0 | 0.2 |

In Fig. 13 a sensitivity study is performed for the ELS mode II tests by varying the interface strength $\sigma_{t,II}$, which is computed from the predefined set of values for $\delta_{II,c}$ and $k$. The fracture toughness is kept constant at $G_{II,c} = 5\,N/mm$. All results may be considered equally acceptable. Thus, it is not possible from one experiment to determine a unique set of values for $\delta_{II,c}$ and $k$ (and similarly for the corresponding parameters in case of mode I loading) that may be regarded as interface material properties.

## 5. Mixed-mode formulation

The interface element constitutive law, Eq. 4, may be written in terms of a single damage variable $D$, for mode I loading as

$$\sigma_I = \begin{cases} K_{I,0}\delta_I & if \quad D \le 0 \\ (1-D)K_{I,0}\delta_I & if \quad 0 < D < 1 \\ 0 & if \quad D \ge 1 \end{cases} \tag{6}$$

and similarly for mode II. The damage variable is

$$D = 1 - \frac{\delta_0}{\delta}\left[1 - \left(\frac{\delta}{\delta_c}\right)^k\right] \tag{7}$$

where the relative displacements, in case of mixed mode loading, are computed as follows:

- Equivalent mixed-mode relative displacement:

$$\delta = \left( \max\left(\delta_I, 0\right)^{2\alpha} + \left|\delta_{II}\right|^{2\alpha} \right)^{\frac{1}{2\alpha}} \qquad (8)$$

which can be derived [6] from the mixed mode criterion

$$\left(\frac{G_I}{G_{Ic}}\right)^{\alpha} + \left(\frac{G_{II}}{G_{IIc}}\right)^{\alpha} = 1 \qquad (9)$$

in which usually $1 \le \alpha \le 2$.

- Damage initiation threshold - derived from the quadratic strength criterion:

$$\delta_0 = \delta \left\{ \left(\frac{\langle \delta_I \rangle}{\delta_{I,0}}\right)^2 + \left(\frac{\left|\delta_{II}\right|}{\delta_{II,0}}\right)^2 \right\}^{-\frac{1}{2}} \qquad (10)$$

- Equivalent mixed mode relative displacement at failure:

$$\delta_c = \delta \left[ \left(\frac{\langle \delta_I \rangle}{\delta_{Ic}}\right)^{\alpha} + \left(\frac{\left|\delta_{II}\right|}{\delta_{IIc}}\right)^{\alpha} \right]^{-\frac{1}{\alpha}} \qquad (11)$$

which can be derived from Eq. 9., written as

$$\left(\frac{G}{G_c}\right)^{\alpha} = \left(\frac{G_I}{G_{Ic}}\right)^{\alpha} + \left(\frac{G_I}{G_{IIc}}\right)^{\alpha} \qquad (12)$$

## 6. Numerical example

The finite element model of a repaired coupon that was tested experimentally is shown in Fig. 14. The longitudinal cross section is modeled as 2D plane strain problem. Symmetry is taken into account. The plies are modelled by a single layer of orthotropic elements. The top cover plate is modeled by two elements per ply to capture better the edge effects in its tapered part. The 0/90° plies have stiffness of $E_x$=67 *GPa,* the ±45° plies – $E_x$=16 *GPa*. The properties in the *z* direction correspond to the through thickness properties of the laminate. The properties of the interface are those given in Table 1.

The force-displacement response is presented in Fig. 15. The load at failure is predicted to be *maxP*=25.5 *kN* and it is in excellent agreement with the experimental failure loads, which were in the range $P_u$=25.1 *kN* to $P_u$ = 25.8 *kN*.

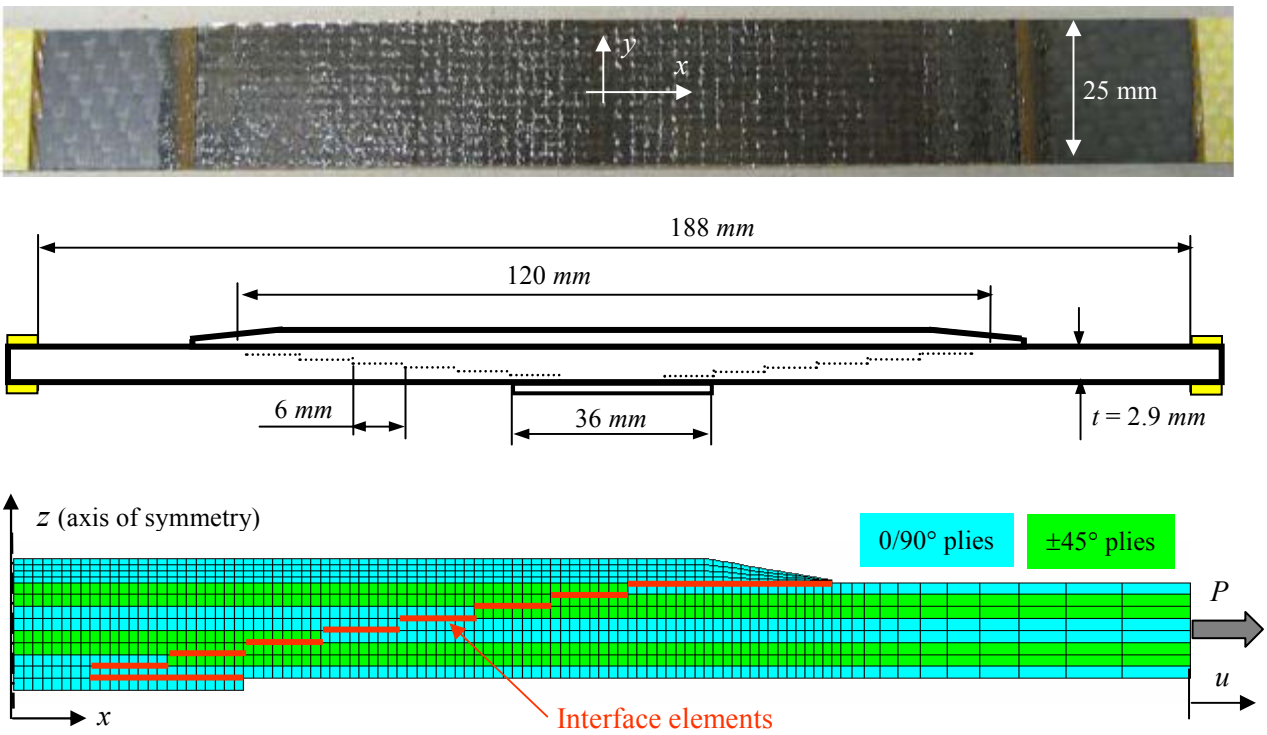


Fig. 14. A repaired coupon: Photo, Schematic cross section; Finite element 2D (half) model.

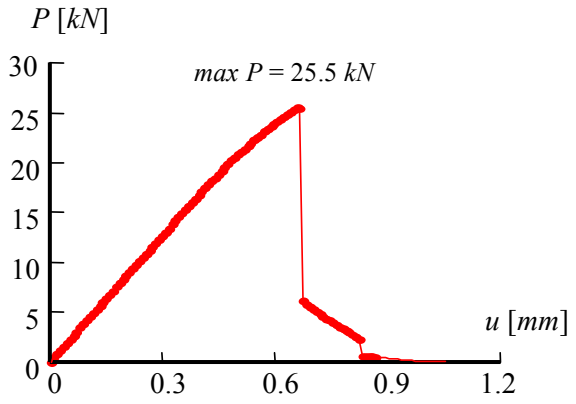


Fig. 15. Force-displacement response.

A sensitivity study is performed by varying the interface decohesive zone parameters that are not determined directly by experiments: $k$ and $\delta_{Ic}$, $\delta_{IIc}$ (or $\sigma_{t,I}$, $\sigma_{t,II}$, which are interrelated via Eq. 5 for a fixed fracture toughness). The critical energy release rates $G_{Ic} = 1.33\ N/mm$ and $G_{IIc} = 5.0\ N/mm$ are kept constant. The results are presented in Fig. 16A, as function of $\delta_{Ic}$, and in Fig. 16B - as function of $k$. The failure load increases with the increase of the interface strength $\sigma_{t,I}$ and $\sigma_{t,II}$ as well as with the decrease of the relative displacement at failure $\delta_{Ic}$ and $\delta_{IIc}$,. It can be seen that the experimental failure load can be predicted by several sets of values for these parameters.

## 5. Conclusions

The mode I and mode II fracture properties of the FM300-2 adhesive bond between 5HS/RTM6 laminates were determined experimentally by DCB and ELS tests, respectively. The fracture toughness in mode I is initially increasing with the increase of the crack length and then converges to a constant value $G_{Ic}$ = 1.33 *N/mm*. In mode II a significant dependence of $G_{IIc}$ on the crack length was observed, which was most probably due to the friction forces and interlocking of the fibre bundles of the cracked rough surfaces. In subsequent numerical analyses a value of $G_{IIc}$ = 5.0 *N/mm* was used.

The crack propagation was studied numerically by means of interface elements based on the decohesive zone model. It was shown that beam theory and FE analyses, using conventional interface constitutive law with linear material degradation, could be used to analyse the steady crack propagation. However, a significant non-linear behaviour was observed before the initiation of the crack propagation, which could only be modelled if a non-linear material degradation was used with an increased magnitude of the interface relative displacement at failure.

An adhesive stepped flush joint was studied experimentally and numerically. A mixed mode interaction criterion was used together with the non-linear material degradation of the interface. The agreement between the experimental and numerical

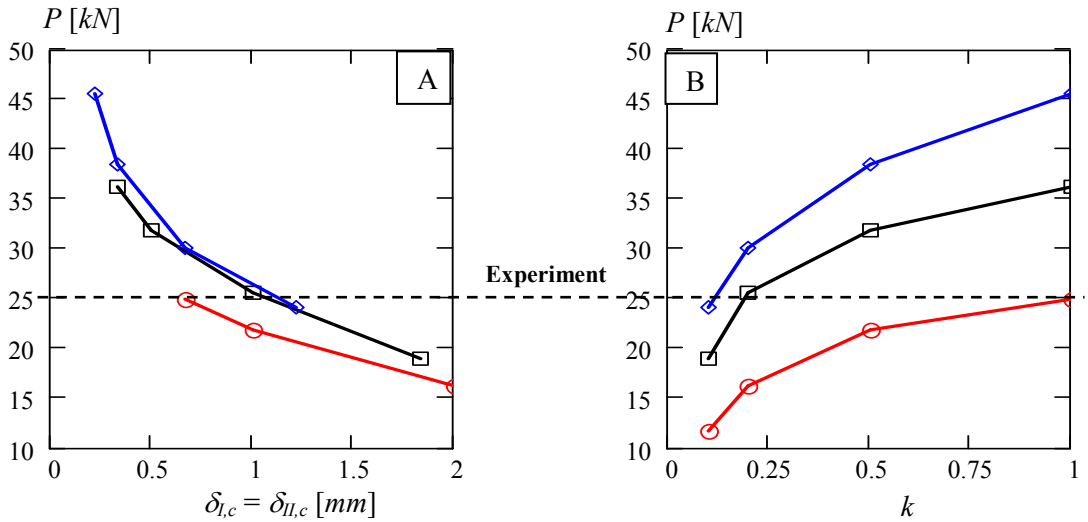


Fig. 16 FE analysis of a repaired coupon. Sensitivity study.

—◇— $\sigma_{t,I} = 12$, $\sigma_{t,II} = 45$; —□— $\sigma_{t,I} = 8$, $\sigma_{t,II} = 30$; —○— $\sigma_{t,I} = 4$, $\sigma_{t,II} = 15$ MPa

results was excellent.

Sensitivity studies were performed to study the influence of the parameters defining the interface non-linear material degradation – $k$, $\delta_{Ic}$, $\delta_{IIc}$. Agreement with the experimental results could be achieved by several sets of parameters. Experimental results for various mode ratios would be required for a unique determination of these parameters.

## 6. References


[1] Tenchev R.T. and Falzon B.G. "Composite adhesive repairs - experimental and numerical analysis of delamination failure". Report ELRIPS-WP7a-ICL-TREP-08, Dept Aeronautics, Imperial College, London, 2007.

[2] Schellekens J.C.J. and de Borst, R. "Free edge delamination in carbon epoxy laminates: a novel numerical/experimental approach". *Comput. Struct.* Vol. 28, pp 357-373, 1993.

[3] William J.G. "On the calculation of energy release rates for cracked laminates". *Int. J. Fracture*. Vol. 36, pp 101-119, 1988.

[4] Davies P., Blackman B.R.K. and Brunner A.J. "Standard test methods for delamination resistance of composite materials: Current status". *Applied Composite Materials* Vol. 5, pp. 345–364, 1998.

[5] Blackman B.R.K., Hadavinia H., Kinloch A.J., Paraschi M. and Williams J.G. "The calculation of adhesive fracture energies in mode I: revisiting the tapered double cantilever beam (TDCB) test". *Engineering Fracture Mechanics*, vol. 70, pp. 233–248, 2003.

[6] Mi Y., Crisfield M., Davies G. and Hellweg H. "Progressive delamination using interface elements". *J. Compos. Mater.* Vol. 32, pp 1246–1272, 1998.

[7] Tenchev R.T. and Falzon B.G. "A pseudo-transient solution strategy for the analysis of delamination by means of interface elements". *Finite Element in Analysis and Design*, Vol 42. pp 698-708, 2006.

[8] Tvergaard V. "Effect of fibre debonding in a wisker-reinforced metal". *Mater. Sci. Eng.*, Vol. 125, pp 203-213, 1990.